Crystal Structure and Mechanism of Catalysis of a Pyrazinamidase from *Pyrococcus horikoshii*†

Xinlin Du,‡,§ Weiru Wang,§ Rosalind Kim,|| Hisao Yakota,|| Huy Nguyen,§ and Sung-Hou Kim*,§,||

Department of Chemistry, University of California, Berkeley, and Physical Biosciences Division, Lawrence Berkeley National Laboratory, Berkeley, California 94720

Received July 24, 2001; Revised Manuscript Received September 26, 2001

ABSTRACT: Bacterial pyrazinamidase (PZAase)/nicotinamidase converts pyrazinamide (PZA) to ammonia and pyrazinoic acid, which is active against *Mycobacterium tuberculosis*. Loss of PZAase activity is the major mechanism of pyrazinamide-resistance by *M. tuberculosis*. We have determined the crystal structure of the gene product of *Pyrococcus horikoshii* 999 (PH999), a PZAase, and its complex with zinc ion by X-ray crystallography. The overall fold of PH999 is similar to that of *N*-carbamoylsarcosine amidohydrolase (CSHase) of *Arthrobacter sp*. and YcaC of *Escherichia coli*, a protein with unknown physiological function. The active site of PH999 was identified by structural features that are also present in the active sites of CSHase and YcaC: a triad (D10, K94, and C133) and a cis-peptide (between V128 and A129). Surprisingly, a metal ion-binding site was revealed in the active site and subsequently confirmed by crystal structure of PH999 in complex with Zn^{2+}. The roles of the triad, cis-peptide, and metal ion in the catalysis are proposed. Because of extensive homology between PH999 and PZAase of *M. tuberculosis* (37% sequence identity), the structure of PH999 provides a structural basis for understanding PZA-resistance by *M. tuberculosis* harboring PZAase mutations.

Pyrazinamide (PZA),[1] an analogue of nicotinamide, is an important first line drug for tuberculosis (TB) (*1*). The addition of PZA to isoniazid and rifampin allows the conventional 9-month tuberculosis treatment to be shortened to 6 months (*2*). These three drugs form the cornerstone for initial tuberculosis therapy as recommended by the Centers for Disease Control and Prevention (*3*) and short course treatment by the World Health Organization (*4*). PZA-resistance by *Mycobacterium tuberculosis* is highly correlated with mutations in its *pnc*A gene, which encodes pyrazinamidase(PZAase)/nicotinamidase activity (*5*−*11*). These mutations impair the ability of PZAase to hydrolyze PZA to ammonia and pyrazinoic acid (Figure 1), which is the active form of PZA because of its ability to inhibit fatty acid synthetase (FASI) of *Mycobacterium tuberculosi* (*12*). The physiological function of nicotinamidase is to convert nicotinamide to nicotinic acid and ammonia (Figure 1) in the pyridine nucleotide cycle (*13*). The structural similarity between nicotinamide and PZA allows the same enzyme to hydrolyze PZA.

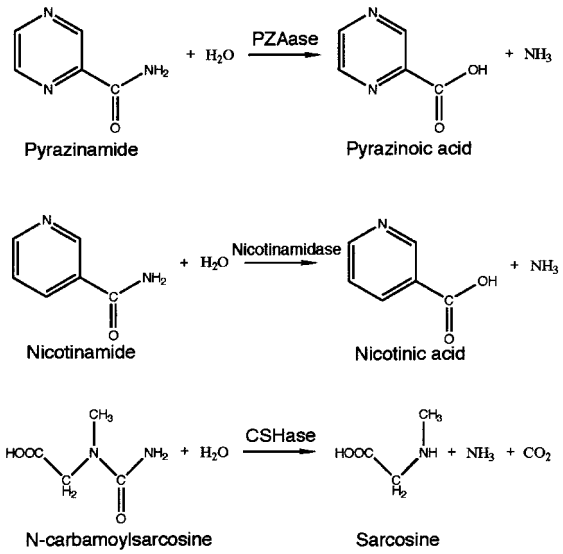

FIGURE 1: Reactions catalyzed by PZAase, nicotinamidase, and CSHase.

The gene product of *Pyrococcus horikoshii* 999 (PH999) has extensive sequence homology (37% sequence identity) to the *M. tuberculosis* pyrazinamidase. We have expressed PH999 in *Escherichia coli* and solved its three-dimensional structure by X-ray crystallography. The structure of PH999 revealed a potential metal ion-binding site in the active site. We were able to confirm that Zn^{2+} increases the pyrazinamidase activity of PH999 and obtained the structure of its complex with Zn^{2+}. Here we report the three-dimensional structure of *P. horikoshii* pyrazinamidase at 2.05 Å resolution and the structure of its complex with Zn^{2+} at 1.65 Å resolution.

† This work was supported by the Director, Office of Science, Office of Biological and Environmental Research, of the U.S. Department of Energy under Contract DE-AC03-76SF00098.

* To whom correspondence should be addressed. Phone: (510) 486-4333. Fax: (510) 486-5272. E-mail: shkim@cchem.berkeley.edu.

‡ Current address: Howard Hughes Medical Institute, University of Texas, Southwestern Medical Center, 5323 Harry Hines Blvd., Dallas, TX 75390.

§ Department of Chemistry.

|| Physical Biosciences Division.

[1] Abbreviations: PZA, pyrazinamide; PZAase, pyrazinamidase; TB, tuberculosis; PH, *Pyrococcus horikoshii*; DTT, dithiothreitol; MAD, multiple-wavelength anomalous dispersion; CSHase, *N*-carbamoylsarcosine amidohydrolase; YcaC, gene product of *yca*C of *E. coli*; DCase, *N*-carbamoyl-D-amino acid amidohydrolase.

10.1021/bi0115479 CCC: $20.00
Published on Web 10/31/2001

MATERIALS AND METHODS

Bacterial Expression, Purification, and Crystallization of PH999. The subcloning of PH999 from *Pyrococcus horikoshii* genome was carried out according to the "sticky-end PCR" method (*14*). Two pairs of primers were used to produce two PCR products, which were mixed, heated, and cooled to produce a DNA fragment with NdeI and BamHI sticky ends, which was in turn inserted into pET21a (*15*). The protein was expressed in a methionine auxotroph, *E. coli* strain B834 (DE3)/SJS1244 (*16*, *17*), that was grown in M9 medium supplemented with selenomethionine. Native protein was expressed in the same strain grown in LB medium. In the purification process, the cell lysate was subjected to heating (80 °C for 30 min), anion-exchange (HiTrap-Q, Pharmacia), and size-exclusion (Superdex 75, Pharmacia) column chromatography. To avoid potential oxidation of the protein, 10 mM DTT was used in all buffers. The initial crystallization conditions were screened with a sparse matrix sampling method (*18*) (Hampton Research, CA) using hanging drop vapor diffusion method at room temperature. Needle clusters of native protein were obtained in condition 10 of Hampton Research Crystal Screen (100 mM sodium acetate, pH4.6, 200 mM ammonium acetate, 30% PEG 4000). Diffraction quality crystals were obtained by microseeding a drop consisting of 1 μL of 20 mg/mL PH999 in 20 mM Tris-HCl, pH 7.5, 1 mM EDTA, and 1 μL of 100 mM sodium acetate, pH 4.6, 250 mM ammonium acetate, 22.5% PEG 3350. It was critical that seeding be performed 1 h after vapor equilibration. The same crystallizing condition and seeding technique yielded only long needle crystals for the selenomethionine derivative of PH999. Addition of 8% glycerol and increasing the PEG concentration to 27.5% in the crystallization solution greatly improved the quality of selenomethionine crystals. Crystals of native protein in complex with Zn^{2+} were grown in mother liquor containing 100 mM sodium acetate, pH 4.6, 250 mM ammonium acetate, 5 mM $ZnCl_2$, 8% glycerol, and 27.5% PEG 3350.

Measurement of PZAase Activity. The assay for pyrazinamidase activity was carried out according to Wayne's procedure (*19*) with some modifications. In the reaction, 20 mM PZA was first incubated with 50 μM PZAase in 50 mM sodium phosphate, pH 6.5, 10 mM DTT. At various time intervals, 100 μL aliquots of the reaction and 10 μL of 20% $FeNH_4(SO_4)_2$ were added to 890 μL of 100 mM Gly-HCl (pH 3.4) and OD_{480} was immediately measured. Since the K_m of pyrazinamidase is expected to be less than 1 mM (*20*), the activity measured in this way is k_{cat} of PZAase. The activity was found to be 17.3 and 357 μmol of PZA hydrolyzed/mg of PZAase/minute at room temperature or at 60 °C, respectively. These numbers are comparable to the values reported for other pyrazinamidases (*20*, *21*). When the assay was carried out in the presence of 2 mM $ZnSO_4$ at room temperature, k_{cat} increased 19-fold to about 333 μmol/mg/minute.

Structure Determination. The three-wavelength diffraction data of 1.9 Å was collected on a selenomethione derivative crystal at the Stanford Synchrotron Radiation Laboratory (SSRL) beam line 1-5. Data collection was carried out under cryogenic conditions with the crystal being protected by 10% glycerol in mother liquor. All data sets were processed with DENZO (*22*) and reduced with SCALEPACK (*22*) and programs in CCP4 package (*23*). The SeMet crystal was in space group $P2_1$ with unit cell dimensions of $a = 59.1$ Å, $b = 43.3$ Å, $c = 66.1$ Å, $\beta = 112.1°$. The structure was solved by multiple-wavelength anomalous dispersion (MAD) phasing method (*24*). Program SOLVE (*25*) was used to locate the **6** selenium sites in the asymmetric unit and to calculate initial phases which were further improved by solvent flattening, NCS averaging, and histogram matching with program DM in CCP4 package. Each asymmetric unit contained two monomers and two models were built using the program O (*26*). However, the models could not be refined successfully against the data set at remote wavelength. Specifically, *R* factors could only be lowered to 0.4 even when the Fourier difference map ($F_o - F_c$) revealed no extra strong density. This may indicate twining of the particular crystal on which the MAD data was collected. The same difficulty was encountered on other crystals with cell dimensions of $a = 59.1$ Å, $b = 43.3$ Å, $c = 66.1$ Å, $\beta = 112.1°$, although the solution was originally obtained in this unit cell. A 2.05 Å data set of native protein and a 1.65 Å resolution data set of PH999−Zn^{2+} complex were collected at SSRL beamline 7-1 and at the Macromolecular Crystallography Facility beamline 5.0.2 at the Advanced Light Source of the E. O. Lawrence Berkeley National Laboratory, respectively. These two crystals were also in $P2_1$ space group but had a unit cell of $a = 33.0$ Å, $b = 43.4$ Å, $c = 55.8$ Å, $\beta = 101.2°$. The molecular replacement solutions for the 2.05 and 1.65 Å (Zn^{2+}−PH999 complex) data sets were obtained by using the structure model obtained from the MAD data set as search model. The two structures reported in this paper were refined against the 2.05 and 1.65 Å (Zn^{2+}−PH999 complex) data sets using SHELX program. The statistics of the data collection, reduction, and refinement is shown in Tables 1 and 2.

Coordinates. The atomic coordinates and structure factors have been deposited into the RCSB protein data bank with accession numbers 1ILW (native structure) and 1IM5 (PH999−Zn^{2+} complex).

RESULTS

Architecture and Topology. A ribbon diagram of PH999 is shown in Figure 2. The secondary structure elements are defined in Figure 3. The structure is comprised of a six-stranded parallel β sheet with helices packed on either side to form an α/β single domain. The strands are arranged in the order 3−2−1−4−5−6 when numbered according to their positions in the primary sequence. Three helices, α2, α3, and α4 are packed against one side of the central sheet while α1 and a long loop preceding β3 are packed against the other face.

Structural Similarities to Other Proteins. The structure of PH999 was compared to the protein structures in the protein data bank (PDB) using the Dali program (*29*). The two proteins with the highest Z scores are *N*-carbamoylsarcosine amidohydrolase (CSHase) of *Arthrobacter sp*. and YcaC of *E. coli*. These two proteins were also identified by PSI−BLAST (*30*) as homologues of PH999. Panels a and b of Figure 4 show superposition of PH999 with CSHase and YcaC, respectively. CSHase hydrolyzes *N*-carbamoylsarcosine to sarcosine, carbon dioxide, and ammonia (Figure

Table 1: Data Collection and Reduction Statistics

	SeMe[a]			native[b]	Zn^{2+} complex[b]
	peak	edge	remote		
wavelength (Å)	0.979 34	0.979 88	0.925 26	1.08	1.0
resolution (Å)	1.9	1.9	1.9	2.05	1.65
no. of unique data	46 760	47 186	47 165	9862	18 049
redundancy	2.60	2.65	2.66	4.246	3.11
completeness[c]	97.3 (82.2)	98.2 (92.7)	98.1 (92.1)	99.2 (88.0)	97.3 (81.9)
$I < 3\sigma(I)$ (%)[c]	24.5 (45.1)	24.7 (48.5)	26.8 (50.1)	13.8 (33.9)	1.5 (4.0)
R_{merge} (%)[c]	4.6 (20.0)	4.8 (19.9)	5.0 (21.9)	2.7 (9.3)	3.6 (6.4)
avg $I/\sigma(I)$[c]	24.3 (5.5)	24.3 (5.9)	23.0 (5.5)	42.5 (17.4)	37.8 (25.5)
mosaicity	0.511	0.511	0.498	0.995	0.505

[a] Space group $P2_1$. Cell: $a = 59.1$ Å, $b = 43.3$ Å, $c = 66.1$ Å, $\alpha = 90.0°$, $\beta = 112.1°$, $\gamma = 90.0°$. Each monomer has three selenomethionines. [b] Space group $P2_1$. Cell: $a = 33.0$ Å, $b = 43.4$ Å, $c = 55.8$ Å, $\alpha = 90.0°$, $\beta = 101.2°$, $\gamma = 90.0°$. Two data sets, with short and long exposure times, were taken on a single crystal and merged together. [c] Data shells 99.0−1.9 (1.93−1.90) Å for the SeMe crystal, 20.0−2.05 (2.09−2.05) Å for native crystal, 20.0−1.65 (1.68−1.65) Å for the crystal of PH999−Zn^{2+} complex.

Table 2: Refinement Statistics

	native data	Zn complex
resolution (Å)	2.05	1.65
no. of reflections used	9761 (98.6%)	17 977 (97%)
no. of reflections for free R	955	1775
R-factor (%)	18.1	15.3
R_{free} (%)	25.7	23.2
rmsd bonds (Å)	0.007	0.008
rmsd angles (deg)	1.6	2.1
no. of waters	88	127
anisotropic *B*-refinement[a]	no	yes
residues in Ramachandran plot (%)[b]		
most favored	92.1	92.1
additional	7.9	7.9
disallowed	0.0	0.0

[a] Anisotropic B refinement was carried out in Shelx. [b] Calculated by PROCHECK (*27*).

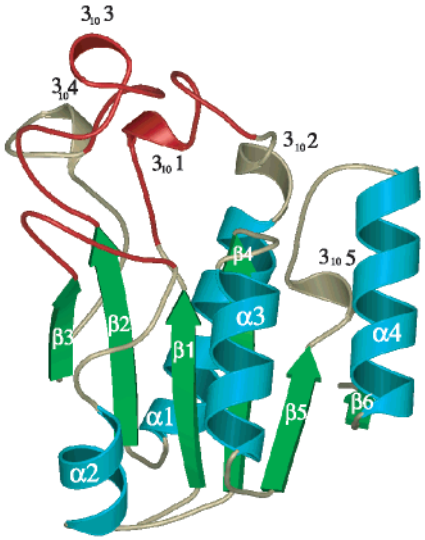

FIGURE 2: Ribbon diagram of PH999. α-Helices and β-strands are color-coded in cyan and green, respectively. The three loops in red (from residues 10 to 21, 128 to 133, and 52 to 72, respectively) contribute most to the scaffold of the active site. Mutations that confer PZA-resistance show some degree of clustering in the corresponding regions of PZAase of *Mycobacterium tuberculosis*.

1) in one of the two alternative pathways for creatine degradation (*31*). YacC is a hydrolase of unknown specificity and physiological function (*32*). The active site of CSHase, which sits on the C-terminal side of the central parallel sheet, has been identified by crystallographic studies on protein crystals treated with aldehyde inhibitors (*31*, *33*). There are indeed big cavities in the corresponding position of YcaC and PH999 structures. Several structural features of the CSHase active site are also conserved in the cavities of PH999 and YcaC. First, there is a triad with similar geometry in the bottom of each cavity. The triad consists of C133, K94, and D10 in PH999, C177, K144, and D51 in CSHase, C118, R84, and D19 in YcaC (Figure 4, panels a, b, and c and Figure 5a). Interestingly, a similar triad (C171, K126, and E46) is present in *N*-carbamoyl-D-amino acid amidohydrolase (DCase), although DCase has a different, four-layer sandwich architecture (*34*). Another conserved feature of the three cavities is the presence of a cis-peptide bond, which is between V128 and A129 in PH999, between A172 and T173 in CSHase, and between V113 and V114 in YcaC, respectively (Figure 4c). The cis-peptide bond is invariably preceded by a glycine (G127, G171, and G112, in PH999, CSHase, and YcaC, respectively) in sequence. Because of the importance of the triad and cis-peptide in the catalytic function of CSHase (*33*), the cavities of PH999 and YcaC are, in all likelihood, active sites as well.

Active Site with Zinc Ion. The active site of PH999 is surrounded by four loops that consist of residues from 10 to 23, 52 to 72, 94 to 103, and 128 to 133, respectively (underlined in Figure 3). Residues that contribute a side chain that lines the active site include D10, F15, L21, V23, D52, H54, S60, W68, H71, K94, A95, E101, A102, Y103, V128, A129, Y132, and C133. The volumes of the active site cavities as calculated by VOIDOO (*35*) are 10.5 and 47.5 $Å^3$ for CSHase and PH999, respectively. While the volume of the cavity in CSHase structure is comparable to the volume of its substrate, the cavity in PH999 is larger than the expected substrate, pyrazinamide. Visual inspection of the 2.05 Å structure revealed a potential metal ion-binding site, which is embedded in the cavity and lined with D52, H54, S60, H58, and H71. Subsequently, it was found that Zn^{2+} increased the k_{cat} of the enzyme by about 19-fold. Other divalent ions tested, including Mg^{2+}, Mn^{2+}, Ca^{2+}, and Cd^{2+}, did not increase the activity. The crystal structure of PH999 grown in the presence of 5 mM $ZnCl_2$ was solved by molecular replacement. A strong peak with 30σ in $F_o - F_c$ map was observed in the expected position and was attributed to Zn^{2+}. The zinc ion is fixed in place by Oδ2 of D52, Nε2 of H54, and Nε2 of H71, and the octahedral coordination is completed by three water molecules, water 203, 214, and

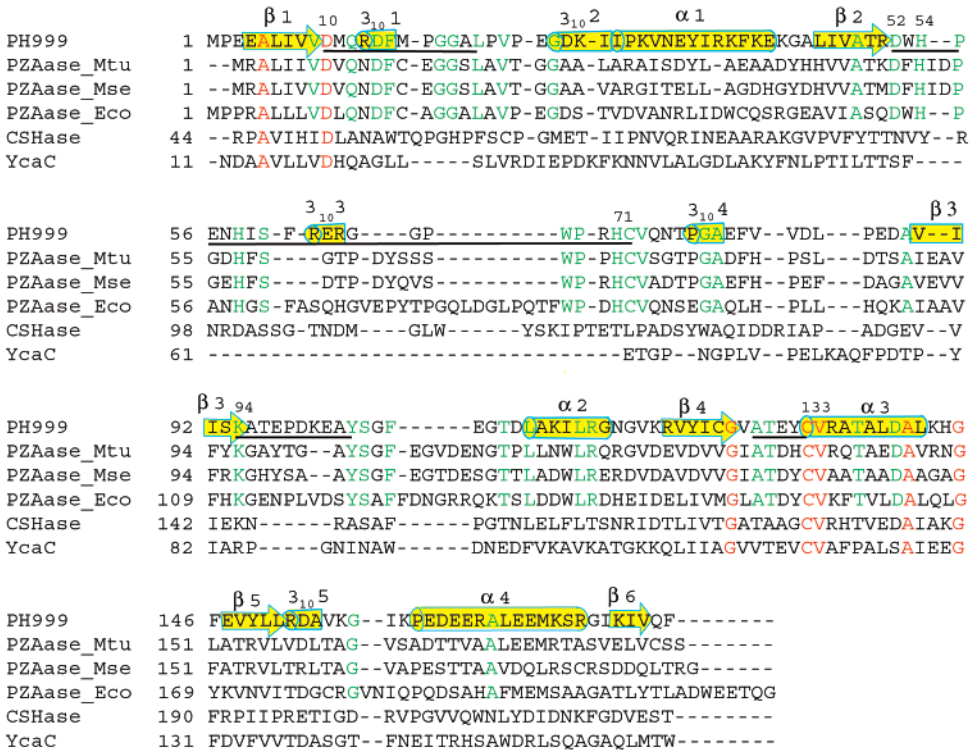

FIGURE 3: Multiple sequence alignment of PH999 (accession number BAA30096), pyrazinamidases of *Escherichia coli* (P21369), *Mycobacterium smegmatis* (AAD11442), and *Mycobacterium tuberculosis* (AAB37768), CSHase (P32400), and YcaC (P21367). The alignment of the four pyrazinamidases was made with PIMA (*28*) program, while the alignment of PH999 with CSHase and YcaC was carried out with Dali (*29*) program. The residues conserved in the pyrazinamidases are colored in green. The residues conserved in all six sequences are colored in red. The residues in the four loops that line the active site are underlined.

223. The isotropic or average isotropic *B* factors of the zinc ion, protein ligands (side chains of D52, H54, and H71), and water ligands (water 203, 214, and 223) are 13.37, 13.07, and 18.63, respectively. These temperature factors compare favorably with the overall *B* factors of 19.28 and 34.65 for protein atoms and water molecules in the final model and indicate that zinc and its ligands are well defined. The triad and Zn^{2+} ion occupy the opposite side of the active sites, leaving a space in the middle for substrate binding. Panels b and c of Figure 5 show the electron density maps of the zinc-binding site and a schematic diagram of the active site with Zn^{2+} ion, respectively. Zinc ions are more commonly observed with tetrahedral coordination, especially in "zinc finger" proteins where they are coordinated by sulfurs that are rather large. However, octahedral coordination of zinc is not rare for oxygen and nitrogen coordination. One of the classic protein examples is zinc insulin that has two distinct octahedral zinc sites (*36*).

DISCUSSION

Mechanism of Catalysis. The conservation of the active-site cysteine, the triad, and the cis-peptide among the homologous proteins suggest that they play important roles in catalysis. The role of the active-site cysteine can be inferred from the biochemical and crystallographic studies on CSHase. CSHase is strongly inhibited by thiol-modifying reagents (*33*). In the crystal structures of CSHase in complex with aldehyde inhibitors, glyoxylic acid, or succinic semialdehyde, C177 is modified by the inhibitors (*33*). Therefore, C177 was proposed to participate in covalent catalysis as a nucleophile, like the nucleophilic cysteine in cysteine proteases (*31*, *33*). By analogy, C133 of PH999 likely attacks the carbonyl carbon of PZA to form an acylated enzyme, which decays to release pyrazinoic acid. The roles of the other two members of the triad are not established, although one of the residues is likely to act as a general base to activate C133. Because the equivalent of K94 is arginine in YcaC, which can hardly act as a general base, we propose that D10, instead of K94, is the general base. D10 adopts two conformations in the structure of PH999 in complex with Zn^{2+}, one of which is ideal for abstracting proton from C133. The exhibition of dual conformations may result from partial protonation of D10 since pH of crystallization condition (4.6) is close to the pK_a of an aspartic acid. K94 is in a position to form an ion pair with either D10 or C133, therefore, stabilizing either the aspartate form of D10 or the thiolate form of C133 in various stages of the catalysis. The thiolate of C133 can be further stabilized by the dipole moment of α3. The direct consequence of forming the cis-peptide is that the amide hydrogen sticks out into the active site and forms a potential oxyanion hole with the amide nitrogen of C133. The oxyanion hole is often observed in the structures of serine proteases, cysteine proteases, and many other hydrolases that utilize a catalytic triad and plays a key role in catalysis by stabilizing the negative charge on the carbonyl oxygen in the transition state and the tetrahedral intermediate. In the structure of PH999 and its complex with Zn^{2+}, the putative oxyanion hole is occupied by a water molecule (Figure 5a), indicating that it is in fact capable of binding an oxygen atom. This hypothesis is further supported by the structures of CSHase in complex with aldehyde inhibitors (*31*). Figures 5 and 6 of the cited paper showed that the

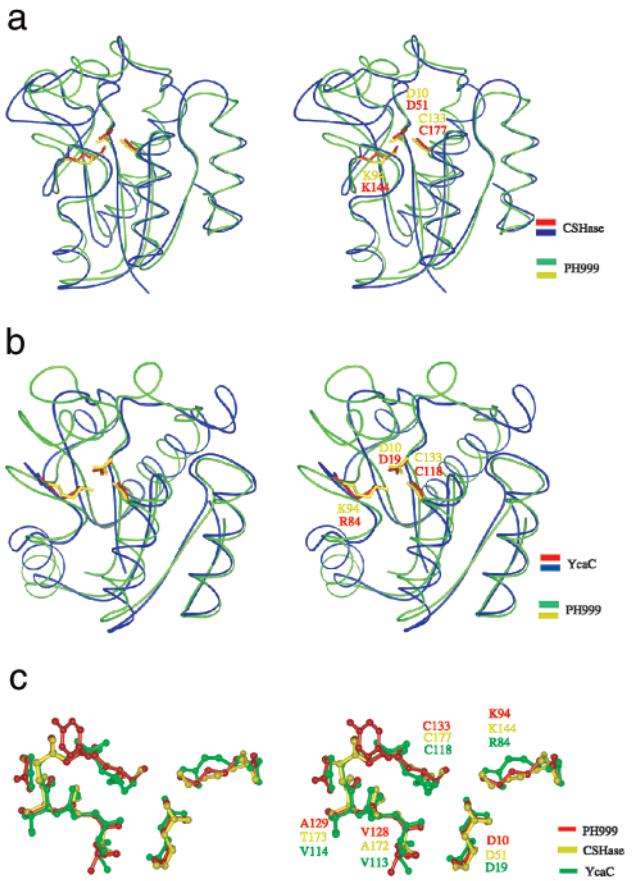

FIGURE 4: (a) Structure alignment of PH999 (green) and CSHase (blue) by Dali (*29*). (b) Structure alignment of PH999 (green) and YcaC (blue). (c) Alignment of selected residues in the active sites of PH999, CSHase, and YcaC. The triad (C133, K94, and D10 in PH999; C177, K144, and D51 in CSHase; C118, R84, and D19 in YcaC) and cis-peptide (between V128 and A129 in PH999; A172 and T173 in CSHase; V113 and V114 in YcaC) are shown.

carbonyl oxygen of the aldehyde does interact with the two amide hydrogens.

The Zn^{2+}-binding site is not present in the CSHase or YcaC structure. However, the residues involved in coordinating Zn^{2+}, D52, H54, and H71 are highly conserved in pyrazinamidases. Therefore, metal ion utilization is likely a general feature of pyrazinamidases. A metal ion may simply stabilize a particular protein conformation or play a direct role in catalysis. There is no structural evidence for the first scenario. The binding of Zn^{2+} induces no detectable conformational change in the backbone structure of PH999, not even in the loop that forms the zinc-binding site (from residue 52 to 71). Enzyme-bound metal ions are known to provide nucleophilic water for catalysis. One of the three Zn^{2+}-bound water molecules, water 214, is 4.6 Å away from C133 in the PH999−Zn^{2+} structure and would have a clear path to attack the carbonyl carbon of the thioester bond in the acylated enzyme. Thus, we propose that the function of the Zn^{2+} ion is to activate water 214 for the hydrolysis of the thioester bond. The increase of k_{cat} by Zn^{2+} is consistent with this proposal.

On the basis of the above discussion, we propose a mechanism for PZA hydrolysis by PZAase as illustrated in Figure 6. The hydrolysis reaction can be largely divided into two halves. In the first half of the reaction, the enzyme is acylated at C133 through a thioester bond. This half involves

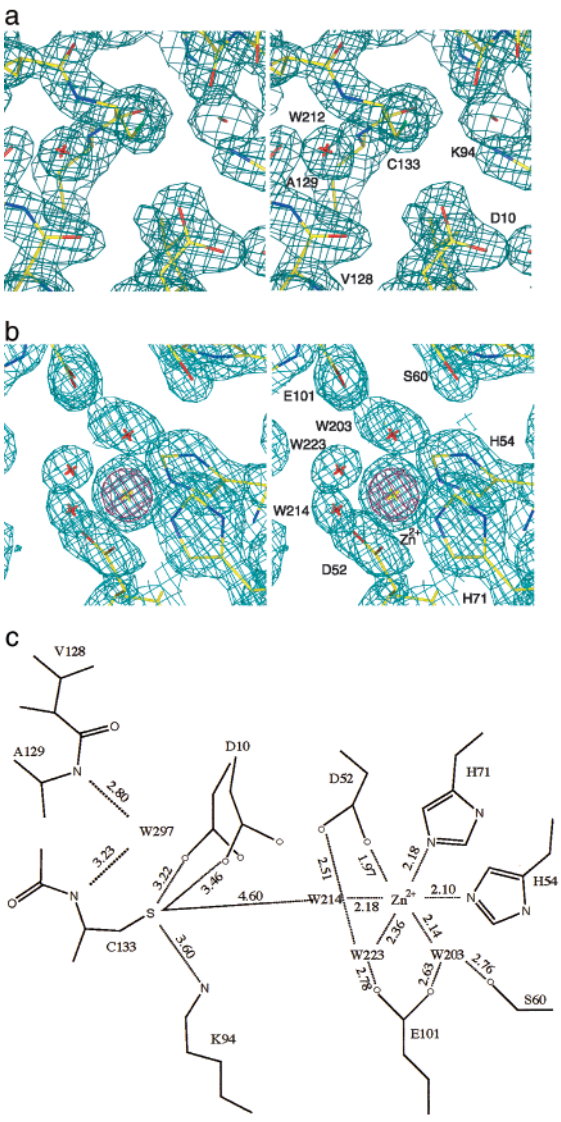

FIGURE 5: (a) 2.05 Å electron density map ($2F_o - F_c$) of PH999 contoured at 1.2σ in the vicinity of C133. (b) 1.65 Å $2F_o - F_c$ map (cyan, contoured at 1.5σ) and $F_o - F_c$ map (magenta, 15σ) calculated with a model without Zn^{2+}. (c) Schematic diagram of Zn^{2+}-bound active site.

(a) PZA binding, (b) the activation of C133 by D10, (c) attack on the carbonyl carbon of PZA by the thiolate of C133, and (d) the decay of the tetrahedral intermediate to release ammonia and generate acylated enzyme. The second half of the reaction involves (e) the attack of zinc-activated water on the carbonyl carbon of the thioester bond, (f) the binding of a water molecule, which (g) replenishes the nucleophilic water and protonate D10, and (h) the decay of the tetrahedral intermediate to release pyrazinoic acid.

Structural Basis for PZA Resistance of M. tuberculosis Carrying PZAase Mutations. The structure of *M. tuberculosis* pyrazinamidase is expected to be very similar to that of PH999. The two proteins share 37% sequence identity. Of the 15 residues that are expected to line the active site based on sequence alignment (Figure 3), only V128 and Y132 of PH999 are not conserved between the two. Therefore, the structure of PH999 should lend insight into the structural basis of loss of PZAase activity observed in PZA-resistant *M. tuberculosis* strains. Studies on these strains have unveiled

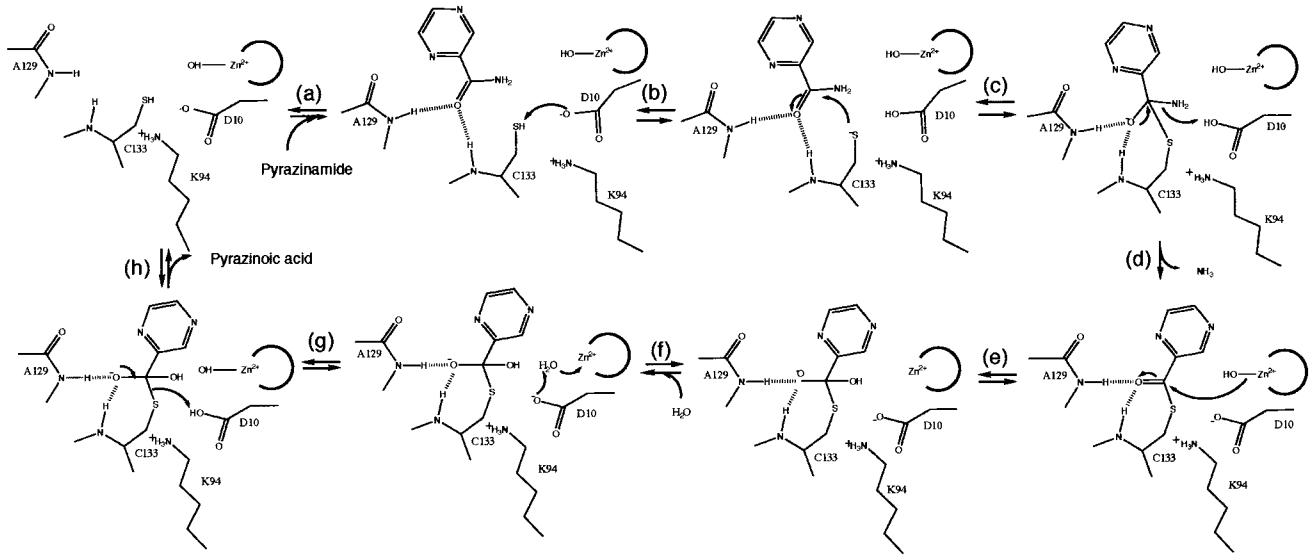

FIGURE 6: Proposed mechanism of PZA hydrolysis by PZAase.

a remarkably wide array of mutations in *M. tuberculosis* PZAase that lead to the loss of pyrazinamidase activity. While these mutations are scattered along the polypeptide chain, some degree of clustering was observed in three regions (*6*, *9*) that correspond to three of the four loops that contribute most to the scaffold of the active site (from 10 to 21, 128 to 133, and 52 to 72 of PH999, colored in red in Figure 2). Some mutations directly modify the active site triad and metal ion-binding site. These include mutations at C138 (equivalent to C133 of PH999), D8 (D10), K96 (K94), D49 (D52), H51 (H54), and H71 (H71). Detrimental mutations were also observed at all other residues that likely line the active site, such as F13 (F15 in PH999), L19 (L21), H57 (H58), W68 (W68), G97 (A95), Y103 (Y103), I133 (V128), A134 (A129), and H137 (Y132). These mutations potentially affect binding or alignment of the PZA and therefore impair PZAase activity. Mutations of Q10 (Q12), D12 (D14), S104 (S104), and T142 (T137) disrupt the hydrogen-bonding interactions between these side chains and main-chain atoms. Loss of PZAase activity observed on many other positions can be attributed to potential perturbation of the active site or disruption of the packing of the protein core.

Sequence Homology to Other Proteins. Homology search was performed over nonredundant protein sequences in the NCBI database with the PSI-BLAST program (*30*). Most homologous proteins identified by PSI-BLAST have not been characterized by biochemical or genetic methods. The characterized proteins include pyrazinamidases of *E. coli* (accession number P21369), *M. smegmatis* (accession number AAD11442), and *M. tuberculosis* (accession number AAB37768), several isochorismatases (2,3 dihydro-2,3 dihydroxybenzoate synthase) of different organisms, as well as CSHase of *Arthrobacter sp*. (P32400) and YcaC of *E. coli* (accession number, P21367). Isochorismatases have low but significant homology (around 25%) with PH999. However, the nucleophilic cysteine is not conserved in the sequences of the isochorismatases and neither are residues D52, H54, and H71, which are involved in the coordination of the metal ion. Therefore, the catalytic mechanism of isochorismatases is likely to be different.

ACKNOWLEDGMENT

We thank Dr. Thomas Earnest for his help in data collection at beam line 5.0.2 of ALS and Dr. Jaru Jancarik for her advice on crystallization experiments. Portions of this research were carried out at the Stanford Synchrotron Radiation Laboratory, a national user facility operated by Stanford University on behalf of the U.S. Department of Energy, Office of Basic Energy Sciences. The SSRL Structural Molecular Biology Program is supported by the Department of Energy, Office of Biological and Environmental Research, and by the National Institutes of Health, National Center for Research Resources, Biomedical Technology Program, and the National Institute of General Medical Sciences.

REFERENCES

1. Konno, K., Feldmann, F. M., and McDermott, W. (1967) *Am. Rev. Respir. Dis. 95*, 461−469.
2. Steele, M. A., and Des Prez, R. M. (1988) *Chest 94*, 845−850.
3. *MMWR Morb Mortal Weekly Rep.* (1993) Vol. 42, pp 1−8.
4. World Health Organization (1995) *WHO Report on the Tuberculosis Epidemic. Stop TB at the source*, Vol. 270, Tuberculosis Programme, Geneva, Switzerland.
5. Scorpio, A., and Zhang, Y. (1996) *Nat. Med. 2*, 662−667.
6. Scorpio, A., Lindholm-Levy, P., Heifets, L., Gilman, R., Siddiqi, S., Cynamon, M., and Zhang, Y. (1997) *Antimicrob. Agents Chemother. 41*, 540−543.
7. Sreevatsan, S., Pan, X., Zhang, Y., Kreiswirth, B. N., and Musser, J. M. (1997) *Antimicrob. Agents Chemother. 41*, 636−640.
8. Hirano, K., Takahashi, M., Kazumi, Y., Fukasawa, Y., and Abe, C. (1997) *Tuberculosis Lung Dis. 78*, 117−122.
9. Lemaitre, N., Sougakoff, W., Truffot-Pernot, C., and Jarlier, V. (1999) *Antimicrob. Agents Chemother. 43*, 1761−1763.
10. Marttila, H. J., Marjamaki, M., Vyshnevskaya, E., Vyshnevskiy, B. I., Otten, T. F., Vasilyef, A. V., and Viljanen, M. K. (1999) *Antimicrob. Agents Chemother. 43*, 1764−1766.
11. Cheng, S. J., Thibert, L., Sanchez, T., Heifets, L., and Zhang, Y. (2000) *Antimicrob. Agents Chemother. 44*, 528−532.
12. Zimhony, O., Cox, J. S., Welch, J. T., Vilcheze, C., and Jacobs, W. R., Jr. (2000) *Nat. Med. 6*, 1043−1047.
13. Neidhardt, F. C. (1987) *Escherichia coli and Salmonella typhimurium: cellular and molecular biology*, American Society for Microbiology, Washington, DC.

14. Zeng, G. (1998) *Biotechniques 25*, 206−208.
15. Studier, F. W., Rosenberg, A. H., Dunn, J. J., and Dubendorff, J. W. (1990) *Methods Enzymol. 185*, 60−89.
16. Leahy, D. J., Hendrickson, W. A., Aukhil, I., and Erickson, H. P. (1992) *Science 258*, 987−991.
17. Kim, R., Sandler, S., Goldman, S., Yokota, H., Clark, A., and Kim, S.-H. (1998) *Biotechnology Lett. 20*, 207−210.
18. Jancarik, J., and Kim, S.-H. (1991) *J. Appl. Crystallogr. 24*, 409−411.
19. Wayne, L. G. (1974) *Am. Rev. Respir. Dis. 109*, 147−151.
20. Boshoff, H. I., and Mizrahi, V. (1998) *J. Bacteriol. 180*, 5809−5814.
21. Guo, M., Sun, Z., and Zhang, Y. (2000) *J. Bacteriol. 182*, 3881−3884.
22. Otwinowski, Z., and Minor, W. (1997) *Methods Enzymol. 276*, 307−327,
23. Dodson, E. J., Winn, M., and Ralph, A. (1997) *Methods Enzymol. 277*, 620−633,
24. Hendrickson, W. A., Horton, J. R., and LeMaster, D. M. (1990) *EMBO J. 9*, 1665−1672.
25. Terwilliger, T. C., and Berendzen, J. (1999) *Acta Crystallogr. Sect. D 55*, 849−861.
26. Jones, A., and Kleywegt, G. (1997) *Methods Enzymol. 277*, 173−208.
27. Laskowski, R. A., MacArthur, M. W., Moss, D. S., and Thornton J. M. (1993) *J. Appl. Crystallogr. 26*, 283−291.
28. Smith, R. F., and Smith, T. F. (1992) *Protein Eng. 5*, 35−41.
29. Holm, L., and Sander, C. (1993) *J. Mol. Biol. 233*, 123−138.
30. Altschul, S. F., Madden, T. L., Schäffer, A. A., Zhang, J., Zhang, Z., Miller, W., and Lipman, D. J. (1997) *Nucleic Acids Res. 25*, 3389−3402.
31. Zajc, A., Romao, M. J., Turk, B., and Huber, R. (1996) *J. Mol. Biol. 263*, 269−283.
32. Colovos, C., Cascio, D., and Yeates, T. O. (1998) *Structure 6*, 1329−1337.
33. Romao, M. J., Turk, D., Gomis-Ruth, F. X., Huber, R., Schumacher, G., Mollering, H., and Russmann, L. (1992) *J. Mol. Biol. 226*, 1111−1130.
34. Nakai, T., Hasegawa, T., Yamashita, E., Yamamoto, M., Kumasaka, T., Ueki, T., Nanba, H., Ikenaka, Y., Takahashi, S., Sato, M., and Tsukihara, T. (2000) *Struct. Folding Des. 8*, 729−737.
35. Kleywegt, G. J., and Jones, T. A. (1994) *Acta Crystallogr., Sect. D 50*, 178−185.
36. Bentley, G., Dodson, E., Dodson, G., Hodgkin, D., and Mercola, D. (1976) *Nature 261*, 166−168.

BI0115479